INTERNATIONAL JOURNAL FOR NUMERICAL AND ANALYTICAL METHODS IN GEOMECHANICS
Int. J. Numer. Anal. Meth. Geomech., **23**, 493–529 (1999)

BIOT CONSOLIDATION ANALYSIS WITH AUTOMATIC TIME STEPPING AND ERROR CONTROL PART 2: APPLICATIONS

SCOTT W. SLOAN[1,*] AND ANDREW J. ABBO[2]

[1] *Department of Civil, Surveying and Environmental Engineering, University of Newcastle, NSW 2308, Australia*
[2] *Formation Design Systems, Fremantle, WA 6160, Australia*

SUMMARY

The automatic time-stepping algorithms developed in a companion paper[1] are used to study the behaviour of several problems involving the consolidation of porous media. The aim of these analyses is to demonstrate that the new procedures are robust, efficient, and can control the global temporal discretization (or time-stepping) error in the displacements to lie near a prescribed error tolerance. Copyright © 1999 John Wiley & Sons, Ltd.

1. INTRODUCTION

The first part of this paper considers the consolidation of porous elastic media. Analyses are performed for the consolidation of a layer under one-dimensional loading, the consolidation of a layer between two rigid plates, and the consolidation of a flexible strip footing resting on a layer of finite depth. In these examples, the performance of the automatic algorithm is investigated using various numbers of coarse time increments and a range of error tolerances. Where appropriate, the efficiency of the automatic algorithm is measured against the efficiency of the conventional backward Euler method by comparing the CPU times required to generate solutions of comparable accuracy. To gauge the ability of the new algorithm to control the level of temporal discretization error, the results from the automatic scheme are compared against those from a second-order accurate scheme using very small time steps. The latter solutions contain negligible temporal discretization errors, and thus serve as useful benchmarks. Note that no attempt is made to measure the spatial discretization error, which is governed by the mesh configuration.

The next part of this paper investigates the ability of the elastoplastic consolidation formulation to predict drained and undrained failure modes in a soil mass. These cases illustrate two extremes of consolidation behaviour and are thus useful checks on the accuracy of the finite element technique. The problems used in these analyses are the expansion of a thick cylinder and the collapse of a flexible strip footing.

* Correspondence to: Scott W. Sloan, Department of Civil, Surveying and Environmental Engineering, University of Newcastle, NSW 2308, Australia

CCC 0363–9061/99/060493–37$17.50

Recived 24 September 1997
Revised 23 January 1998

The final part of the paper considers the consolidation of a flexible strip footing resting on an elastoplastic soil layer. The layer is modelled using a rounded Mohr–Coulomb yield surface with either an associated or a non-associated flow rule. For both the associated and non-associated cases where the dilation angle is non-zero, the automatic time integration procedure is implemented using a Newton–Raphson (or tangent stiffness) iteration scheme to solve the non-linear incremental equations for each time step. For the special case of a non-associated model with a zero dilation angle, an initial stiffness iteration scheme is employed to solve these equations. As in the elastic consolidation examples, the results from the automatic scheme are compared with those from the conventional backward Euler scheme to assess its accuracy and efficiency. These analyses are also used to investigate the effect of the iteration tolerance on the accuracy of the displacements at various stages of consolidation.

In each of the problems to be analysed, whether elastic or elastoplastic, the soil mass is modelled using six-noded triangles with a quadratic displacement expansion for the displacements and a linear expansion for the pore water pressures. This element avoids the spurious oscillations associated with elements which use the same order of expansion for the displacements and pore pressures (see, for example References 2 and 3) and is simple to implement.

For all problems considered in this paper, a ramp loading is imposed over the time period t_0 as shown in Figure 1. Following conventional practice, that rate of loading is frequently expressed in terms of the time factor T_v, rather than the actual time t, since this quantity is dimensionless. In most cases, T_v is defined to be equal to

$$T_v = \frac{c_v t}{H^2}$$

where c_v is a coefficient of consolidation and H is a measure of the length of the drainage path. Note, however, that the coefficient of consolidation may be either one- or two-dimensional, depending on the problem, and the length measure used may also vary. The precise form of T_v will be defined in the preamble to each problem.

To gauge the performance of the automatic time-stepping algorithm, the global temporal errors in the transient displacements $\mathbf{U}_t$ are estimated using the equation

$$u_{\text{error}} = \frac{\|\mathbf{U}_t - \mathbf{U}_{\text{ref}}\|_\infty}{\|\mathbf{U}_{\text{ref}}\|_\infty} \tag{1}$$

where $\mathbf{U}_{\text{ref}}$ are a set of reference displacements calculated at the corresponding time. These reference displacements are computed using the second-order accurate scheme of Thomas and Gladwell,[4] with the three integration parameters set to $\varphi_1 = \varphi_2 = \varphi_3 = 1$. These solutions have a very small temporal discretization error, since they are obtained using a very large number of time increments. Using the reference displacements and equation (1), u_{error} gives an approximate estimate of the global time-stepping error, and may be compared directly against the specified tolerance $DTOL$ to ascertain the performance of the error control strategy. Ideally, the observed value of u_{error} will lie reasonably close to $DTOL$, at least to within an order of magnitude. It is also desirable that, as the tolerance is tightened, the observed time-stepping errors will be reduced by a commensurate amount.

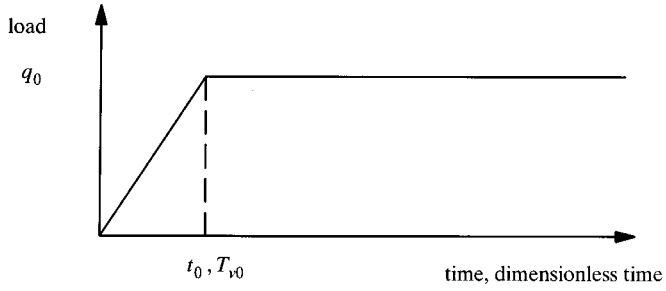

Figure 1. Load versus time

In the results that follow, various timing statistics are given to indicate the efficiency of the proposed automatic time incrementation scheme. All of these are for a Sun Ultra 170 workstation with the Sun FORTRAN 77 compiler and level 3 optimization.

2. ELASTIC CONSOLIDATION

For each of the problems considered in this Section, the soil is modelled as an elastic, isotropic, weightless medium with a uniform permeability. The properties of the soil are thus completely defined by its drained Youngs modulus, E', its drained Poisson's ratio, v', its permeability k, and the unit weight of pore water γ_w.

In all of the elastic analyses, a three-point scheme is used to integrate the element stiffness, coupling and flow matrices for the six-noded triangle. This rule is exact for a straight-sided plane strain triangle with a quadratic expansion for the displacements and a linear expansion for the pore pressures (see, for example, Reference 5) and is the most efficient method available for computing the stiffness and coupling matrices. Note that slightly greater economies could be achieved by employing a one-point rule to evaluate the element flow matrices, **h**, since all of their terms are constants. This was not done in the current study because the additional savings are only marginal.

2.1. One-dimensional consolidation of a finite layer

An analytical solution for the one-dimensional consolidation of an elastic porous layer under a uniform surface pressure has been presented by Terzaghi.[6] The mesh and boundary conditions for this problem are shown in Figure 2. The soil layer is assumed to be of thickness H and loaded by a uniform surface pressure of q_0. As indicated in Figure 1, the finite element analysis assumes that a ramp load is imposed over the dimensionless time period $T_{v0} = 0{\cdot}0001$, where

$$T_{v0} = \frac{c_v t_0}{H^2}$$

and c_v, the one-dimensional coefficient of consolidation, is given by

$$c_v = \frac{kE'(1 - v')}{\gamma_w(1 + v')\ (1 - 2v')} \tag{2}$$

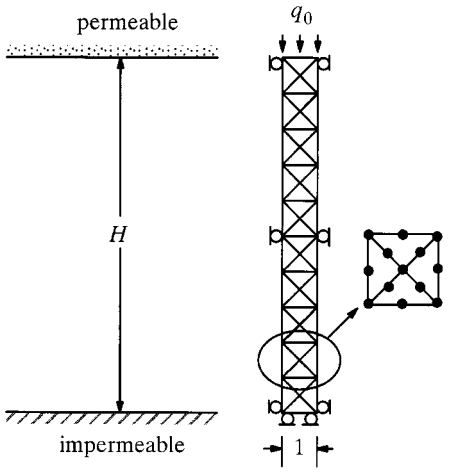

Figure 2. Uniform mesh for one-dimensional consolidation of finite layer

After the total pressure q_0 has been applied over the period T_{v0}, the layer is allowed to consolidate over a dimensionless time factor increment of $\Delta T_v = 1{\cdot}2$. Thus, at the end of the analysis, the total dimensionless time is given by $T_v = 0{\cdot}0001 + 1{\cdot}2 = 1{\cdot}2001$.

To measure the accuracy of various algorithms, the global time-stepping errors in the displacements are estimated using equation (1). The reference displacements for this case are calculated using the second-order accurate scheme of Thomas and Gladwell,[4] with 1000 equal size increments to apply the load and 10,000 equal size time increments to model the subsequent consolidation.

Results for analyses using the automatic time stepping scheme of Sloan and Abbo[1] are shown in Table I, Figures 3 and 4. Data are presented for $DTOL = 10^{-2}$, 10^{-3} and 10^{-4}, which are

Table I. Results for one dimensional consolidation using automatic scheme

DTOL	No. coarse time increments[a]	No. time subincrements[a]		CPU time (s)
		Successful	Failed	
10^{-2}	$1+1=2$	$9+48=57$	$2+3=5$	1·1
	$1+6=7$	$9+50=59$	$2+3=5$	1·5
	$1+12=13$	$9+53=62$	$2+3=5$	1·9
10^{-3}	$1+1=2$	$27+129=156$	$4+3=7$	2·6
	$1+6=7$	$27+133=160$	$4+3=7$	2·9
	$1+12=13$	$27+133=160$	$4+3=7$	3·2
10^{-4}	$1+1=2$	$85+379=464$	$5+3=8$	7·0
	$1+6=7$	$85+382=467$	$5+3=8$	7·3
	$1+12=13$	$85+386=471$	$5+3=8$	7·5

[a]No. in loading stage + No. in consolidation stage = total No.

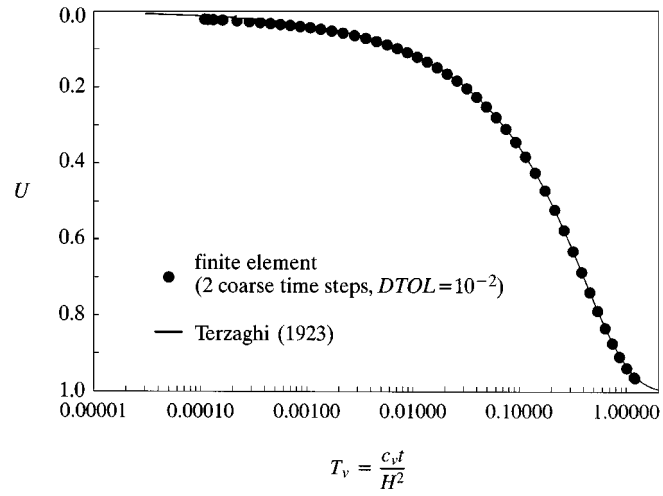

Figure 3. Degree of consolidation versus time factor for one-dimensional consolidation

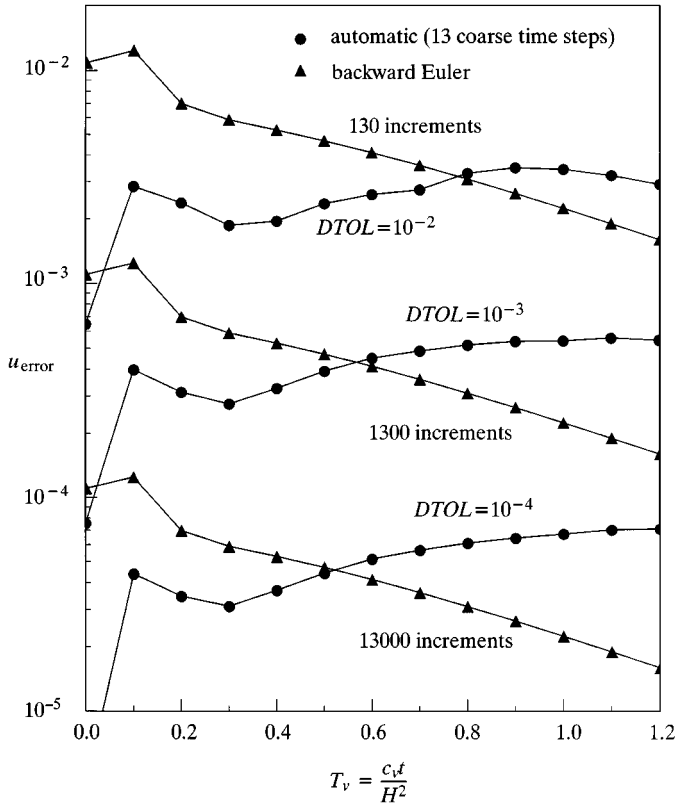

Figure 4. Temporal discretization error in displacements versus time factor for one-dimensional consolidation

typical of the tolerance values that would be used in practice. To test the sensitivity of the automatic scheme to the starting conditions, three runs are performed for each tolerance using 2, 7 and 13 coarse time steps. In each case, all of the load is applied in the first coarse time step which has a time factor increment of $\Delta T_{v0} = 0{\cdot}0001$. The remaining coarse increments are of uniform size and apply a total time factor increment of $\Delta T_v = 1{\cdot}20$. Note that entries in Table I of the form $i + j = k$ indicate that i steps occurred in the loading phase, j steps occurred in the consolidation phase, and k steps occurred overall.

Figure 3 compares the numerical consolidation curve, obtained using the automatic scheme with 2 coarse time steps and $DTOL = 10^{-2}$, against the analytical solution derived by Terzaghi.[6] This analysis generates a total of 57 substeps and its predictions are in excellent agreement with the exact results.

The results in the Table I indicate that, for each value of $DTOL$, the automatic scheme always chooses a similar number of subincrements, regardless of the number of coarse time increments that are specified initially. With $DTOL = 10^{-2}$, for example, the automatic scheme selects 57, 59 and 62 time substeps when 2, 7, and 13 coarse time steps are specified. Each of these analyses automatically selects 9 substeps during the loading phase. Because of the design of the algorithm, it is usual for the last substep in each coarse time step to be truncated. For a fixed value of $DTOL$, this causes the total number of substeps to increase slightly as the number of coarse steps is increased. For all values of $DTOL$, the number of failed substeps is a small proportion of the total number of successful substeps. This suggests that the adaptive substepping strategy is correctly tuned and does not suffer from spurious oscillations.

The variation of the temporal discretization error during each of the automatic analyses with 13 coarse time increments is shown in Figure 4. In each case, the maximum temporal discretization errors are just below the specified tolerance $DTOL$. With $DTOL = 10^{-3}$, for example, the maximum temporal error occurs at $T_v \approx 1{\cdot}0$ and is approximately equal to 5×10^{-4}. These results suggest that the automatic scheme is able to constrain the global time-stepping error to lie near the specified tolerance $DTOL$. Because the automatic scheme increases the step size as consolidation takes place, the temporal error in the displacements is roughly constant over the last-half of the time interval.

To assess the performance of a traditional solution method, this problem was also analysed using the backward Euler scheme with various numbers of equal-size time increments. Since the material is elastic, the backward Euler method requires only two assemblies and two factorizations of the global equations to complete each analysis. These assemblies and factorizations occur at the start of the loading and consolidation phases. The CPU times and temporal discretization errors for the various backward Euler runs are shown, respectively, in Table II and Figure 4.

Table II. Backward Euler results for one-dimensional consolidation

No. time increments			CPU time (s)
Loading	Consolidation	Total	
10	120	130	1·4
100	1200	1300	4·2
1000	12 000	13 000	34

The results in Table II suggest that, for the analyses with up to around a thousand time steps, the bulk of the computational work occurs in the assembly and factorization stages and the CPU time is not proportional to the number of time steps used. For the runs with very small time steps, the assembly and factorization times are less dominant and the overall CPU time grows in the manner expected. Figure 4 indicates that the temporal discretization error in the displacements decreases as the number of time increments is increased. For all the backward Euler analyses, the temporal discretization error in the displacements is greatest at $T_v \approx 0{\cdot}01$ and drops off significantly in later stages of consolidation. The runs with 130, 1300 and 13,000 time steps give maximum time-stepping errors in the displacements of roughly $1{\cdot}2 \times 10^{-2}$, $1{\cdot}2 \times 10^{-3}$ and $1{\cdot}2 \times 10^{-4}$. These results clearly exhibit the first-order accuracy of the backward Euler scheme.

The efficiency of the backward Euler and the automatic schemes can be compared using the data in Tables I and II and Figure 4. Inspection of the latter indicates that the 1300 increment backward Euler analysis gives a maximum temporal discretization error which is close to that of the automatic analysis with $DTOL = 10^{-3}$. The data in Tables II and I reveal that the CPU times for these two runs are, respectively, 4·2 and 3·2 s. For the most accurate analysis with $DTOL = 10^{-4}$, the automatic scheme generates a total of 471 substeps and requires a maximum of 7·5 s of CPU time. This compares very favourably with the 13 000 increment backward Euler run, whose result is of similar accuracy but uses 34 s of CPU time.

The analyses shown in Table I which use just one coarse time increment for the loading phase and one coarse time increment for the consolidation phase are included to highlight the robustness of the proposed algorithm. A bar chart of the successful substeps chosen by the automatic scheme, for the case of $DTOL = 10^{-2}$, is presented in Figure 5. This indicates that the time step grows by almost five orders of magnitude, from an initial value of $T_v \approx 5 \times 10^{-6}$ to a maximum of $T_v \approx 0{\cdot}17$. As expected, the automatic scheme selects very small increments in the early stages of the analysis where the rate of pore pressure dissipation is the greatest. Using a log–log plot of the increment size ΔT_v vs T_v, the growth in step size for all of the automatic runs is shown in Figure 6. The dramatic increases indicated in this plot highlight the inefficiency of

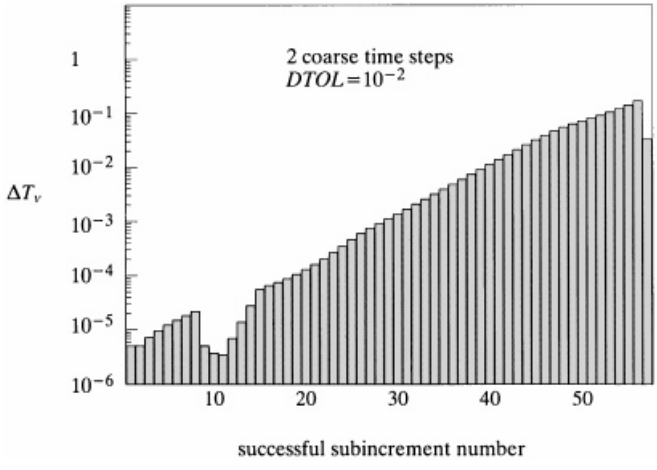

Figure 5. Subincrement size selection for analysis of one-dimensional consolidation

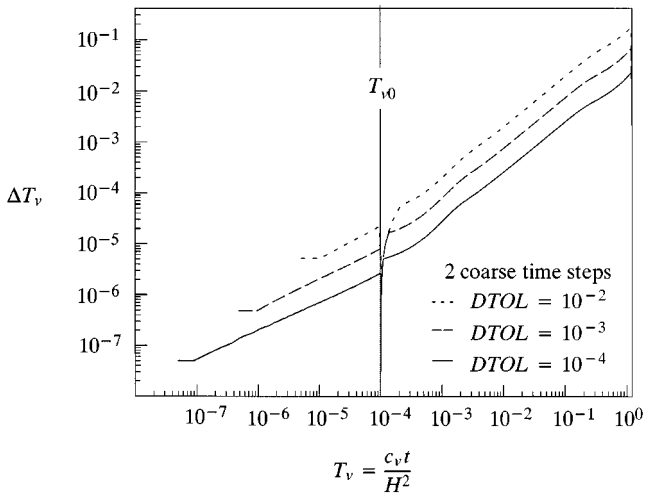

Figure 6. Subincrement size versus time factor for analysis of one-dimensional consolidation

using uniform time steps for this particular problem, and further demonstrates the benefits obtained by the use of an adaptive integration scheme.

A number of researchers, including Reed,[2] and Kanok-Nukulchal and Suaris,[3] and Sandhu *et al.*,[7] have noted that the use of a small initial time step may produce spatial oscillations in the pore pressures near free draining boundaries. Because of this phenomenon, Vermeer and Verrujit[8] recommend that the step size should not be reduced below a threshold value. Using an uncoupled diffusion model for one-dimensional consolidation, they proposed that the minimum time step is given by $\Delta t^{\min} = l^2/(6\theta c_v)$, where l is the length of the shortest element immediately adjacent to a free draining boundary, c_v is the one-dimensional coefficient of consolidation given by equation (2), and θ is an integration parameter. This relation may also be written in the dimensionless form

$$\Delta T_v^{\min} = \frac{1}{6\theta}\left(\frac{l}{H}\right)^2 \tag{3}$$

and is applicable to any one-dimensional element with a linear pore pressure expansion. It should be stressed that (3) is not strictly valid for coupled Biot consolidation problems in one or more dimensions. Vermeer and Verrujit[8] suggest, however, that similar relationships will hold for these cases and give some numerical evidence to support their claim.

Although the practice of using large time steps in the early stages of consolidation may help to reduce the pore pressure oscillations, it will also have the undesirable effect of increasing the temporal discretization error in the solution. This error tends to dissipate as consolidation nears completion, but may be very significant during, and immediately after, the loading phase. Large pore pressure oscillations which are adjacent to free draining boundaries can, alternatively, be viewed as a signal that the mesh needs to be refined in these zones. Indeed, for most practical problems, judicious refinement of the mesh near free draining boundaries will often drastically reduce troublesome oscillations. This is believed to be a better strategy than imposing an artificially large time step constraint on the solution process, since it addresses the cause of the

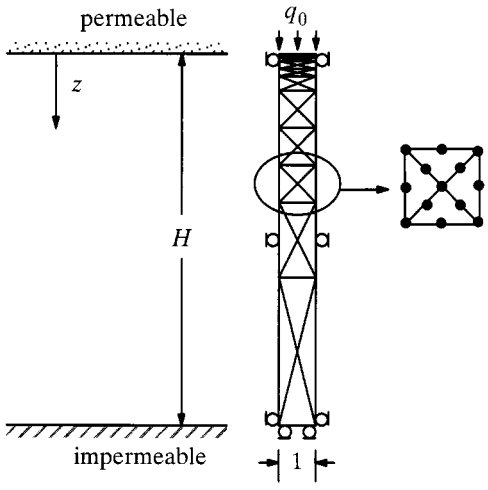

Figure 7. Graded mesh for one-dimensional consolidation of finite layer

oscillations directly and does not introduce additional sources of error. In view of these arguments, the automatic time incrementation schemes developed in Sloan and Abbo[1] do not impose a minimum value on the size of the time step.

To illustrate the effect of mesh refinement on the pore pressures throughout a one-dimensional layer, consider the uniform mesh of Figure 2 and the graded mesh of Figure 7. Both of these grids have the same number of elements and the same number of degrees of freedom, the only difference is that the latter mesh is highly refined in the vicinity of the top drainage boundary. The pore pressure isochrones for these two meshes, obtained from the automatic scheme with $DTOL = 10^{-2}$ and two coarse time steps, are presented in Figure 8. Also shown on this plot are the exact solutions derived by Terzaghi.[6] For the uniform mesh, oscillations in the pore pressures are clearly evident in the very early stages of the analysis but dissipate quickly with time. The oscillations are most pronounced at the end of the loading phase, where $T_v = 10^{-4}$, and arise in spite of the fact that nine time subincrements have been used up to this point. It is interesting to note that these observations are in accordance with equation (3), which predicts that oscillations will occur for the uniform mesh if $\Delta T_v \leqslant 4{\cdot}167 \times 10^{-4}$. The results for the graded mesh are in excellent agreement with Terzaghi's exact solution, even for small values of T_v. This analysis uses 40 time subincrements during the dimensionless time period of $T_v = 10^{-4}$, with the first (and smallest) being equal to $\Delta T_v = 0{\cdot}36 \times 10^{-7}$. Although this value is smaller than the minimum of $\Delta T_v^{\min} = 1{\cdot}042 \times 10^{-6}$ predicted by equation (3), any oscillations in the pore pressures are now small and dissipate extremely quickly.

2.2. *Consolidation of finite layer compressed between two rigid plates*

Consider the consolidation of an elastic plane strain layer, compressed between two smooth rigid plates, as shown in Figure 9. This problem has been solved analytically by

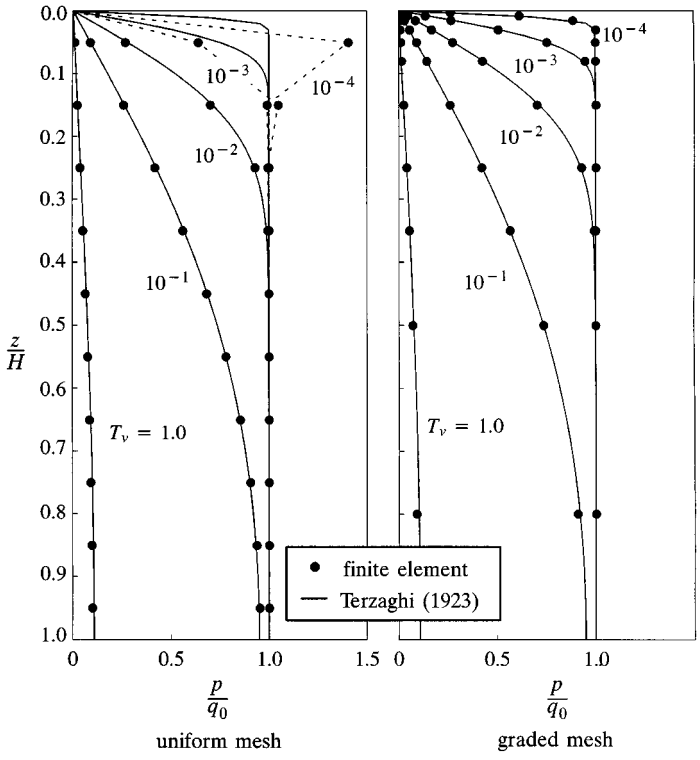

Figure 8. Pore pressure isochromes for one-dimensional consolidation

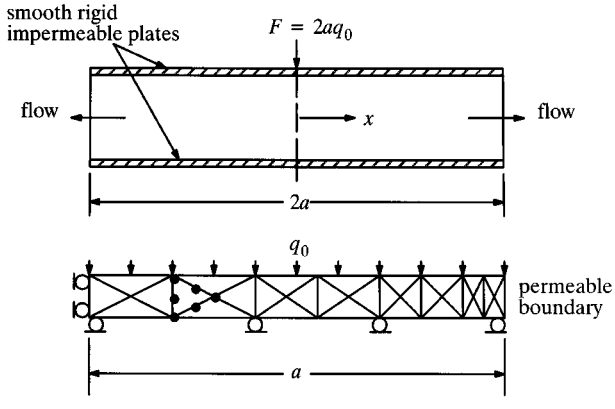

Figure 9. Consolidation of layer between two rigid plates[9]

Mandel,[9] and thus serves as a useful benchmark for checking two-dimensional finite element formulations. In the finite element model of Figure 9, load is applied to the plates in the form of prescribed pressures and the rigid boundary is modelled by constraining

the nodal displacements along the plate interface to be equal. The dimensionless time factor for this problem is

$$T_v = \frac{c_v t}{3a^2}$$

where a is the half-width of the plates and c_v is the one-dimensional coefficient of consolidation defined by (2). The load is ramped, as illustrated in Figure 1, and reaches its maximum value after the dimensionless time period $T_{v0} = 0{\cdot}001$. Once the total pressure, q_0, is applied, consolidation is analysed over a dimensionless time factor increment of $\Delta T_v = 1{\cdot}0$. Therefore, at the conclusion of the analysis, the dimensionless time is given by $T_v = 0{\cdot}001 + 1{\cdot}000 = 1{\cdot}001$.

The reference solution for this example, which provides a benchmark to compute the global time-stepping errors for various other runs, is found using the second-order scheme of Thomas and Gladwell.[4] To ensure that the temporal error is minimised, 1000 and 10,000 equal size increments are used over the loading and consolidation phases, respectively.

Results for the automatic time incrementation scheme are shown in Table III. Data are presented for $DTOL$ values ranging from 10^{-2} to 10^{-4}, with each tolerance being run using 2, 6 and 11 coarse time increments. In each analysis, all of the load is applied in the first coarse time step which has a time factor increment of $\Delta T_v = 0{\cdot}001$. The remaining coarse increments are of uniform size and give a total time factor increment of $\Delta T_v = 1{\cdot}0$. The results in Table III indicate that the behaviour of the automatic scheme is largely independent of the coarse time steps that are specified initially. For a fixed value of the tolerance $DTOL$, it always chooses a similar number of subincrements. With $DTOL = 10^{-2}$, for example, the automatic scheme selects 24, 27 and 30 time substeps when 2, 6, and 11 coarse time steps are specified. Note that no subincrementation is required with this tolerance during the loading phase, as each of the analyses generates only a single substep. As in the one-dimensional consolidation example, the number of failed substeps is a small proportion of the total number of successful substeps.

A typical plot of the transient pore pressure variation at the centre of the layer is shown in Figure 10. This particular curve was obtained using two coarse time increments and a tolerance of $DTOL = 10^{-2}$. With these settings, the finite element analysis generates a total of 24 successful substeps and predicts pore pressures which are in excellent agreement with the exact results of Mandel.[9] A detailed bar chart of the time steps that were used to construct Figure 10 is shown in Figure 11.

Table III. Results for consolidation of layer between rigid plates using automatic scheme

$DTOL$	No. coarse time increments	No. subincrements		CPU time (s)
		Successful	Failed	
10^{-2}	$1+1=2$	$1+23=24$	$0+1=1$	1·2
	$1+5=6$	$1+26=27$	$0+1=1$	1·5
	$1+10=11$	$1+29=30$	$0+1=1$	1·9
10^{-3}	$1+1=2$	$9+60=69$	$4+2=6$	3·0
	$1+5=6$	$9+61=70$	$4+2=6$	3·3
	$1+10=11$	$9+64=73$	$4+2=6$	3·6
10^{-4}	$1+1=2$	$30+173=203$	$5+3=8$	7·9
	$1+5=6$	$30+174=204$	$5+3=8$	8·2
	$1+10=11$	$30+178=208$	$5+3=8$	8·6

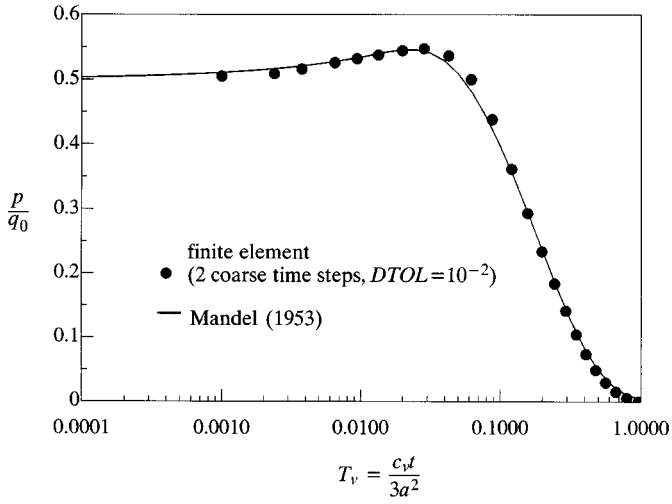

Figure 10. Pore pressure (at centre of layer) versus time factor for consolidation of layer between rigid plates

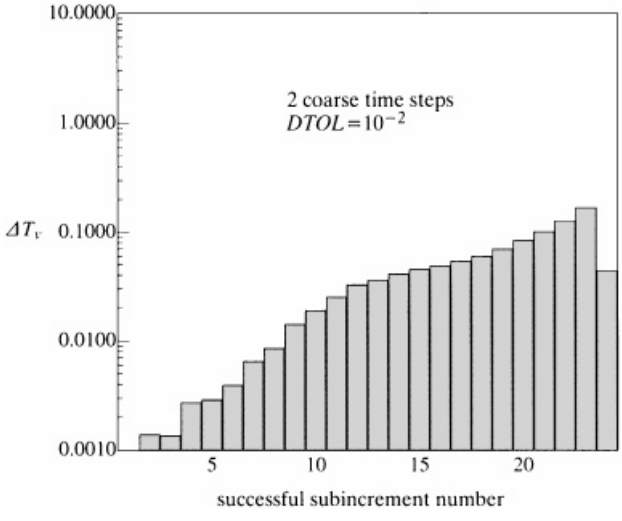

Figure 11. Subincrement size selection for consolidation of layer between rigid plates

Figure 12 illustrates the temporal discretization errors at various stages of the runs with 11 coarse time increments. In each case, the maximum temporal discretization error is just below the specified tolerance $DTOL$ and is roughly constant for the last-half of the consolidation period. With $DTOL = 10^{-3}$, for example, the maximum temporal error occurs at $T_v \approx 0{\cdot}6$ and is approximately equal to 6×10^{-4}. These results again suggest that the automatic scheme is able to constrain the global time-stepping error to lie near the specified tolerance $DTOL$.

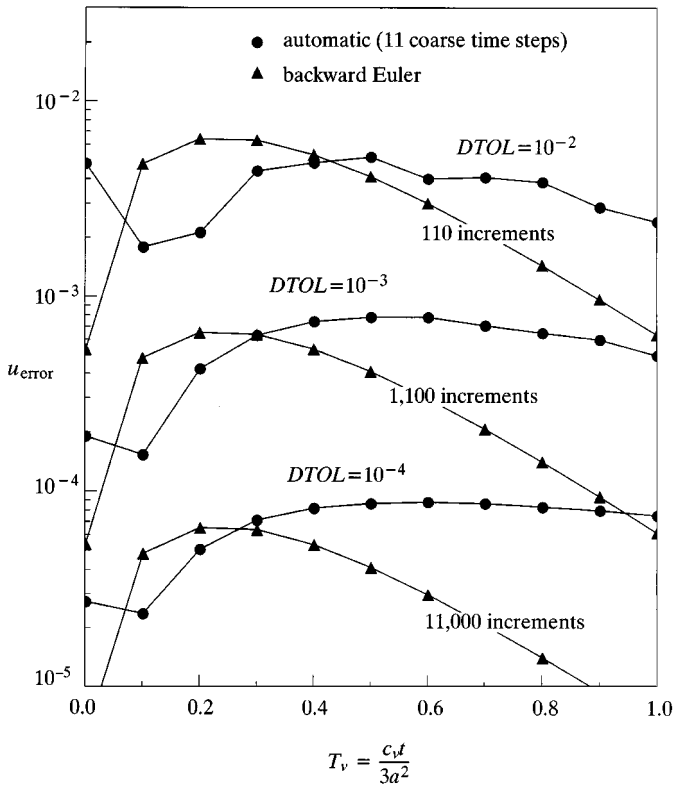

Figure 12. Temporal discretization error in displacements versus time factor for consolidation of layer between rigid plates

To investigate the performance of a traditional solution scheme, this problem was also analysed using the backward Euler algorithm with various numbers of equal size time increments. The CPU times and temporal discretization errors for these runs are shown, respectively, in Table IV and Figure 12. These results confirm the expected first-order accuracy of the backward Euler scheme. For the runs with 110, 1100 and 11,000 uniform increments, the corresponding maximum temporal errors are of the order of 10^{-2}, 10^{-3} and 10^{-4}, respectively.

Table IV. Backward Euler results for consolidation of layer between rigid plates

No. time increments			CPU time (s)
Loading	Consolidation	Total	
10	100	110	1·0
100	1000	1100	3·6
1000	10 000	11 000	30

The relative efficiency of the automatic and backward Euler method can be estimated using the data in Tables III and IV and Figure 12. For example, with $DTOL = 10^{-3}$, the maximum time-stepping error for the automatic analysis is roughly equal to that for the 1100 increment backward Euler analysis. The CPU times for these two runs are very similar, but the automatic scheme achieves this accuracy with a maximum of 73 substeps. For higher accuracies, the efficiency of the automatic scheme increases relative to that of the backward Euler method.

2.3. *Consolidation of flexible strip footing on finite layer*

In this section the automatic time-stepping scheme is used to analyse the consolidation of a rough flexible strip footing resting on a porous elastic layer. The mesh and boundary conditions for the problem considered are shown in Figure 13. In this example, the ramp load is applied to the footing over the initial period $T_{v0} = 0{\cdot}0001$ and the time factor is given by

$$T_v = \frac{c_v t}{H^2}$$

where H is the depth of the soil layer and c_v is the one-dimensional coefficient of consolidation defined by (2). To study the behaviour of the automatic and backward Euler schemes under fully drained conditions, the consolidation process is modelled up to a time factor of $T_v = 10$. This guarantees a fully drained state, as all of the excess pore pressures have essentially dissipated when $T_v \approx 2$.

The reference displacements in this case are calculated differently to the preceding examples, with 1000 equal size time increments being used to model the loading phase and 900 uniform increments per log cycle being used to model the consolidation phase. Since $T_v = 10$ at the end of the analysis, the total number of increments employed in computing the reference solutions is equal to $1000 + 5 \times 900 = 5500$. The efficiency of using a logarithmic incrementation scheme is discussed in more detail later in this section.

Results for various footing analyses with the automatic scheme are shown in Table V. Data are presented for $DTOL$ values ranging from 10^{-1} to 10^{-4}, with each tolerance being run using

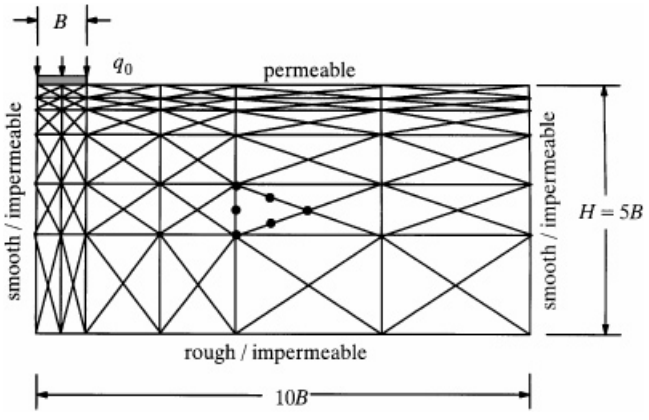

Figure 13. Flexible strip footing on elastic layer

Table V. Results for elastic strip footing using automatic scheme and uniform coarse time increments

$DTOL$	No. coarse time increments[a]	No. time subincrements[a]		CPU time (s)
		Successful	Failed	
10^{-1}	$1+1=2$	$1+19=20$	0	5·0
	$1+5=6$	$1+22=23$	0	5·9
	$1+10=11$	$1+25=26$	0	7·4
10^{-2}	$1+1=2$	$3+36=39$	$2+1=3$	9·1
	$1+5=6$	$3+39=42$	$2+1=3$	9·9
	$1+10=11$	$3+42=45$	$2+1=3$	11·5
10^{-3}	$1+1=2$	$12+89=101$	$3+3=6$	20
	$1+5=6$	$12+91=103$	$3+3=6$	21
	$1+10=11$	$12+95=107$	$3+3=6$	23
10^{-4}	$1+1=2$	$39+247=286$	$4+3=7$	53
	$1+5=6$	$39+250=289$	$4+3=7$	55
	$1+10=11$	$39+253=292$	$4+3=7$	56

2, 6 and 11 coarse time increments. For all analyses, the load is applied in the first coarse time step which has a time factor increment of $\Delta T_{v0} = 0{\cdot}0001$. The remaining coarse increments are of near uniform size and advance the solution to $T_v = 10$. As in previous examples, these results indicate that the automatic scheme chooses a similar number of substeps for each value of $DTOL$, regardless of the initial coarse time step size. With $DTOL = 10^{-2}$, for example, the new algorithm generates 39, 42 and 45 substeps for runs with 2, 6 and 11 initial coarse time steps. The bulk of these substeps occur in the consolidation phase, with only three substeps being generated during the application of the load.

To illustrate the accuracy of the automatic scheme, Figure 14 shows a plot of the degree of consolidation at the centre of the footing versus the time factor for the run with two coarse time steps and $DTOL = 10^{-2}$. The finite element prediction matches the analytic solution of Booker[10] over all of the loading range, with the small amount of deviation indicated being attributable to the spatial discretization error. It is interesting to note that, on the scale of Figure 14, the results for the most stringent tolerance of $DTOL = 10^{-4}$ are indistinguishable from those for $DTOL = 10^{-2}$. This suggests the latter value is a practical starting point for analysing the behaviour of elastic two-dimensional consolidation problems. To gain some insight into the step selection philosophy of the automatic scheme, Figure 15 shows the successful time step sizes for the analysis with $DTOL = 10^{-2}$. As in previous examples, the step size is small at the start of the analysis and increases consistently throughout the entire consolidation process. The step size ranges from a minimum value of $\Delta T_v = 3 \times 10^{-5}$ to a maximum of $\Delta T_v = 3{\cdot}32$ and, on average, grows by an order of magnitude over 6 or 7 consecutive substeps.

To further investigate the step control behaviour of the automatic algorithm, an additional set of footing analyses are performed in which each log cycle of the time factor is used as a single coarse time step. The coarse time steps adopted in these analyses are shown in Table VI. As before, all of the load is imposed over the interval $T_{v0} = 0{\cdot}0001$ and the total time factor at the

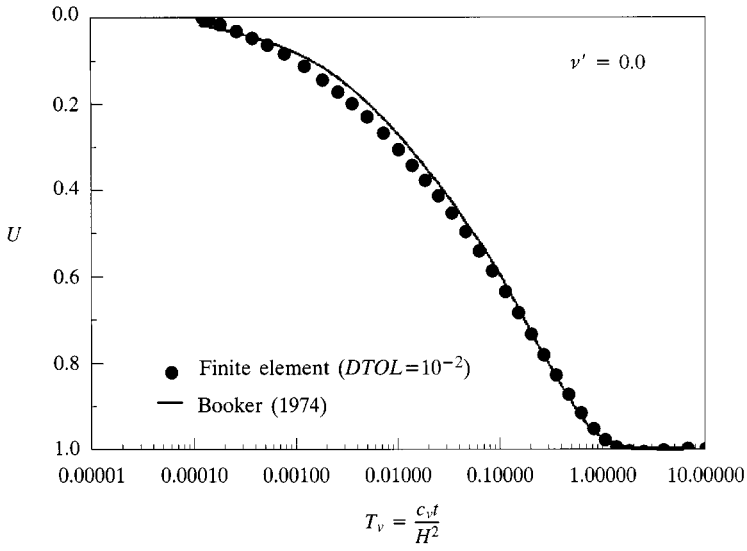

Figure 14. Degree of consolidation versus time factor for elastic strip footing

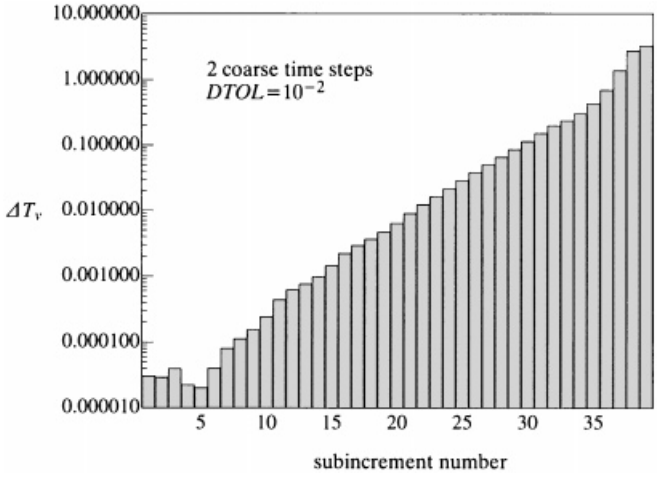

Figure 15. Subincrement size selection for consolidation of elastic strip footing

end of the run is $T_v = 10$. It is pleasing to note that the results of these computations, shown in Table VII, are very similar to those generated using uniform coarse steps (Table V). With $DTOL = 10^{-2}$, for example, an average of 42 substeps are generated in the analyses with uniform coarse steps, while 43 substeps are generated by the analysis with logarithmically varying coarse steps. This reinforces the conclusion from the previous examples that the automatic step control mechanism is largely insensitive to the starting conditions.

Table VI. Log cycles for analysis of strip footing

	Time factor increment (ΔT_v)	Total time factor (T_v)
Loading	0·0001	0·0001
Consolidation	0·0009	0·001
	0·009	0·01
	0·09	0·1
	0·9	1·0
	9·0	10·0

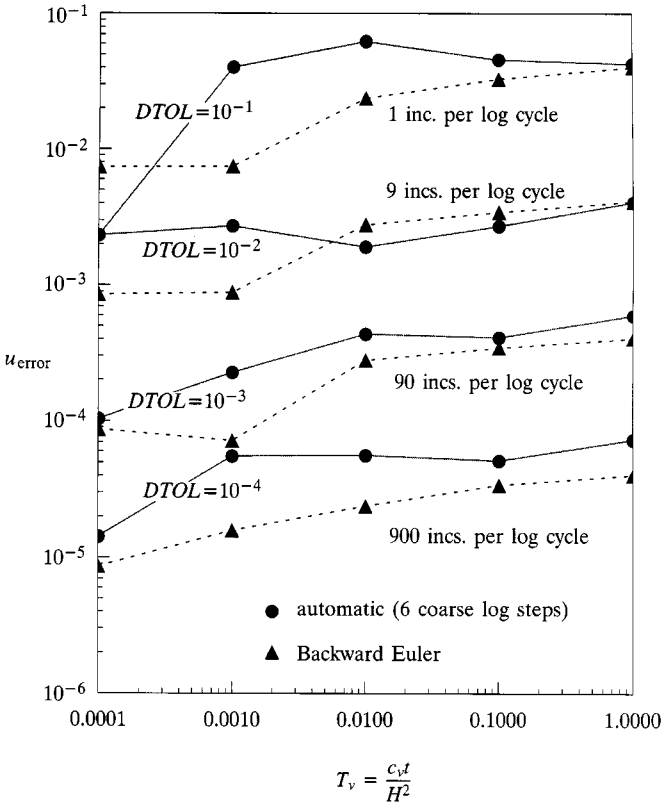

Figure 16. Temporal discretization error in displacements versus time factor for elastic strip footing (logarithmic coarse time steps)

Figure 16 shows the temporal discretisation errors at various stages of the runs with the logarithmic coarse time step variation. These results are plotted only up to $T_v = 1$, as beyond this point the fully drained state is approached and the errors become very small. For all cases, the maximum temporal discretization errors are held just below the specified tolerance $DTOL$ and

Table VII. Results for elastic strip footing using automatic scheme and logarithmic coarse time steps

DTOL	No. coarse time incs. per log cycle	No. subincrements		CPU time (s)
		Successful	Failed	
10^{-1}	1	$1+23=24$	0	6·7
10^{-2}	1	$4+39=43$	$2+2=4$	11·7
10^{-3}	1	$13+94=107$	$3+3=6$	26
10^{-4}	1	$40+258=298$	$4+3=7$	68

Table VIII. Backward Euler results for elastic strip footing using logarithmic increment sizes

No. time increments per log cycle		Total No. time increments	CPU time (s)
Loading	Consolidation		
1	1	$1+5=6$	2·6
9	9	$9+45=54$	3·2
90	90	$90+450=540$	11
900	900	$900+4500=5400$	87

are roughly constant over much of the consolidation period. These results confirm that the automatic scheme is able to constrain the global time-stepping error to a desired level for the case of logarithmically varying coarse time steps.

To gauge the performance of a traditional solution method, the footing problem was also analysed using a backward Euler scheme with a fixed number of increments over each log cycle of the time factor. Although this strategy leads to abrupt changes in step size between adjacent log cycles, it provides a simple hand method for increasing the time increments as consolidation proceeds. To assess the performance of such a scheme the backward Euler algorithm was run with the time step regimes shown in Tables VI and VIII. In these analyses, the loading and consolidation stages were modelled using 1, 9, 90 and 900 increments per log cycle of the time factor. The CPU times and error data for these runs are shown in Table VIII and Figure 16, respectively. The error plots in the latter indicate that the backward Euler scheme, when used with a logarithmic step size variation, gives time-stepping errors which are essentially constant over most of the consolidation period.

In comparing the performance of the two strategies, it can be seen from Figure 16 that the backward Euler run with nine fixed size time increments per log cycle is of comparable accuracy to the automatic analysis with six coarse log steps and $DTOL = 10^{-2}$. For this case, the backward Euler algorithm is over three times faster than the automatic scheme. The automatic scheme, however, is much more competitive for runs where greater accuracy is required. The analysis with six coarse steps and $DTOL = 10^{-4}$, for example, is only marginally less accurate than the backward Euler analysis with 900 increments per log cycle, but uses 22 per cent less CPU time.

3. ELASTOPLASTIC CONSOLIDATION

In this Section, a range of elastoplastic consolidation problems is considered. The overall aim of the studies is to assess the efficiency and accuracy of the non-linear consolidation algorithm developed in Reference 1. In each of the problems discussed, the soil is again modelled as a weightless medium so that the total pore pressure is equal to the excess pore pressure. An elastic perfectly plastic model is assumed for the soil skeleton, and is used in conjunction with the rounded Mohr–Coulomb yield surface described in Abbo and Sloan.[11] Unless noted otherwise, the elastoplastic constitutive laws are integrated using the explicit stress integration scheme described in Reference 12 with a stress error tolerance of $STOL = 10^{-6}$ and a yield surface tolerance of $FTOL = 10^{-9}$. These tolerances are set stringently for the purposes of error checking and benchmarking, and should be relaxed for practical computations. Setting $STOL = 10^{-3}$ and $FTOL = 10^{-6}$ will provide sufficient accuracy in most applications and will also lead to substantial reductions in CPU time.

In all of the elastoplastic analyses, a six-point integration scheme is used to evaluate the element stiffness, coupling, and flow matrices, This rule is used in preference to the three-point rule because it improves the stability of the tangent stiffness iteration algorithm when large plastic strain increments are encountered. Further efficiencies in this area could be realized by using a three-point scheme for the coupling matices and a one-point scheme for the flow matrices.

As described in Reference 1, the non-linear equations which govern elastoplastic consolidation are solved using either an initial stiffness or a Newton–Raphson iteration algorithm. Because the latter proved to be unstable for some problems involving elastoplastic soil with a non-associated flow rule and a zero dilation angle, the initial stiffness algorithm is generally employed for these cases. Unless stated otherwise, the initial stiffness and Newton–Raphson schemes are used with iteration tolerances of $ITOL = 10^{-3}$ and 10^{-6}. The looser tolerance is needed for the initial stiffness scheme because of its much slower rate of convergence. In solving the non-linear equations for each time step, no restriction is placed on the maximum number of iterations that can be performed. This results in the time step size being governed completely by the local error estimator, so that the global time-stepping error in the displacements is due solely to the step control mechanism used in the automatic scheme. Under these circumstances, the global time-stepping errors may be compared directly against the specified error tolerance, $DTOL$, to ascertain the performance of the error control strategy. Note that for practical computations which are not concerned with benchmarking, $MAXITS$ would typically be set in the range 5–10 to avoid significant numbers of wasted iterations.

3.1. Drained and undrained expansion of thick cylinder

Drained and undrained loading conditions represent extremes of consolidation behaviour and can be used to validate finite element models. For real soils, these two modes of deformation are caused, respectively, by extremely slow and extremely fast loading rates. In this context, the terms 'slow' and 'fast' have different meanings for different materials and need to be defined relative to the soil permeability.

Following Reference 13, the drained and undrained predictions of an elastoplastic consolidation formulation may be verified by using exact analytical solutions for the expansion of a thick

cylinder of soil. Under undrained loading, the cylinder deforms at constant volume and its behaviour corresponds to that of an elastoplastic Tresca material. The complete load-deformation response and internal stress distribution for this condition has been given by Hill.[14] More recently, the fully drained analytical solution, which assumes a Mohr–Coulomb material and contains the Hill solution as a special case, has been presented by Yu.[15] As discussed in detail by Small,[13] the material properties for the two different types of loading are not independent and must satisfy the relations

$$E_u = \frac{3E'}{2(1+\nu')} \tag{4}$$

$$c_u/c' = 2\sqrt{N_\phi}/(1+N_\phi) \tag{5}$$

where the subscript u denotes an undrained quantity and

$$N_\phi = (1+\sin\phi)/(1-\sin\phi)$$

These equations, together with the incompressibility condition, govern the parameters that must be used in the Hill solution when it is compared to the undrained consolidation results obtained with a fast loading rate. It is also important to note that the undrained consolidation analysis must be performed with a zero dilation angle in order to avoid large strength gains which are caused by excessive dilatancy.

The geometry, boundary conditions, and axisymmetric finite element mesh used to model the thick cylinder are shown in Figure 17. The drained parameters assumed in the finite element study are

$$E'/c' = 200, \quad \nu' = 0{\cdot}0, \quad \phi' = 30^\circ, \quad \psi' = 0^\circ$$

Equations (4) and (5), together with the constant volume condition, give the undrained parameters required for the Hill solution as

$$E_u/c_u = 346{\cdot}4, \quad \nu_u = 0{\cdot}49999, \quad \phi_u = 0^\circ, \quad \psi_u = 0^\circ$$

For this set of material properties, the drained and undrained collapse pressures of the cylinder are given, respectively, by the expressions $q/c' = 1{\cdot}02$ and $q/c' = 1{\cdot}2$ (or $q/c_u = 1{\cdot}4$), where q is the uniform pressure applied to the inner surface of the cylinder.

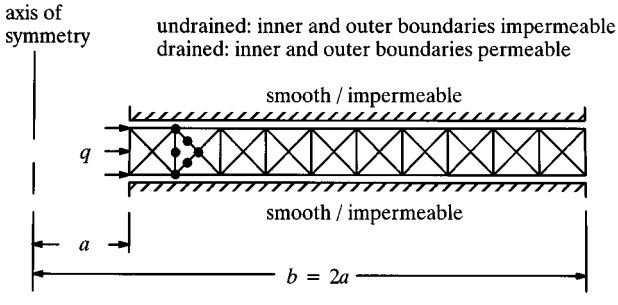

Figure 17. Expansion of thick cylinder

To account for the effects of the soil permeability, the rate at which the load is imposed on the cylinder is defined in terms of the dimensionless quantity

$$\omega = \frac{\Delta q/c'}{\Delta T_v}$$

$$\Delta T_v = \frac{c_v \Delta t}{a^2}$$

In the above equation, c_v is the usual one-dimensional consolidation coefficient and a is the internal radius of the cylinder.

To compute the time-stepping error in the displacements for the various consolidation runs, a set of reference displacements was computed for both the drained and undrained analyses. These were found using the second order method of Thomas and Gladwell[4] with 10 000 equal size time increments and a Newton–Raphson iteration tolerance of $ITOL = 10^{-8}$.

In the first set of analyses, the automatic algorithm is used to predict the undrained response of the thick cylinder. These runs impose a rapid loading rate of $\omega = 10^4$ to simulate undrained conditions and use the Newton–Raphson iteration scheme to solve the incremental equations for each time step. As shown in Table IX, results are generated for analyses using 1 and 10 coarse time steps with error tolerances of $DTOL = 10^{-2}$, 10^{-3} and 10^{-4}. In all cases, the automatic algorithm selects a similar number of subincrements for analyses performed with the same displacement tolerance. With $DTOL = 10^{-2}$, for example, the runs with 1 and 10 coarse time steps generate, respectively, 18 and 23 successful subincrements. Similarly, for a tolerance of $DTOL = 10^{-3}$, the analyses employs 56 and 63 successful subincrements.

The relatively high number of failed subincrements for this example is a consequence of the fact that the undrained deformation response of the cylinder is particularly sensitive to the effects of material at Gauss points turning plastic. Because of the abrupt change in behaviour that is imposed by an elastic perfectly plastic model, an elastic–plastic transition for a single Gauss point has pronounced affect on the value of the local error indicator for this particular problem. This impacts on the present scheme as consecutive substeps are allowed to double in size to enable rapid growth of the time step during later stages of the consolidation process. One possible strategy for reducing the number of failed substeps is to limit this growth factor to a lower value of around 10 per cent. Since most of the failed steps will occur during application of the load, this restriction would not need to be enforced during the consolidation phase. Note, however, that other examples considered later in this paper do not exhibit such a large proportion of failed steps, so this refinement has not been incorporated in the present algorithm.

The data in Table IX indicates that, on average, only two or three iterations are required for each successful substep of the automatic scheme. This reflects the ability of the Newton–Raphson algorithm to provide rapid convergence when used with an appropriate time step. As expected, the maximum number of iterations for a given analysis is highest for cases where the maximum load is applied in a single coarse time step. Somewhat surprisingly, the average number of iterations for a failed step is fairly low and typically lies somewhere between two and three.

The load displacement curve for the undrained analysis with a single coarse time increment and a displacement tolerance of $DTOL = 10^{-2}$ is plotted in Figure 18. Although this is a particularly

Table IX. Results for undrained loading of thick cylinder using automatic scheme and uniform coarse increments

DTOL	No. coarse time increments	No. subincrements		No. iterations			CPU time (s)
		Successful	Failed	Successful[a] steps	Failed[a] steps	Max[b]	
10^{-2}	1	18	10	50	40	7	2·19
	10	23	6	62	20	4	2·51
10^{-3}	1	56	18	129	53	7	3·94
	10	63	21	141	58	3	4·70
10^{-4}	1	250	95	496	198	7	13·9
	10	248	100	494	203	3	14·4

[a] No. iterations in successful or unsuccessful time steps.
[b] Max no. iterations in successful or unsuccessful time steps.

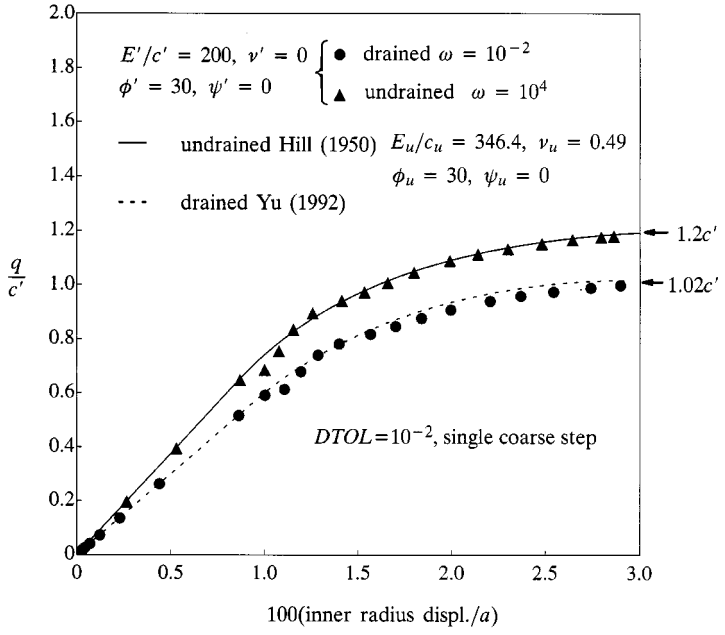

Figure 18. Pressure versus displacement for drained/undrained loading of thick cylinder

severe test, the algorithm successfully reduces and then adjusts the subincrement size to reflect the load-displacement behaviour of the cylinder. The numerical results match the analytical solution of Hill[14] with acceptable accuracy over all of the loading range and predict the exact collapse pressure precisely. The small oscillations which occur upon initial yielding of the cylinder may be eliminated by using a tighter value of *DTOL*. A detailed picture of the subincrement sizes adopted by the automatic algorithm for this example is shown in Figure 19. As expected, the algorithm

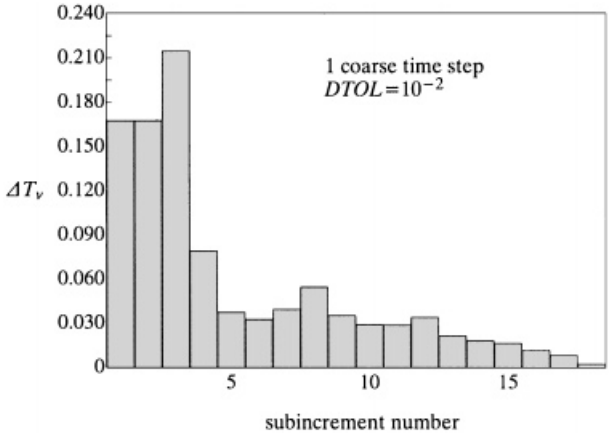

Figure 19. Subincrement size selection for undrained loading of thick cylinder

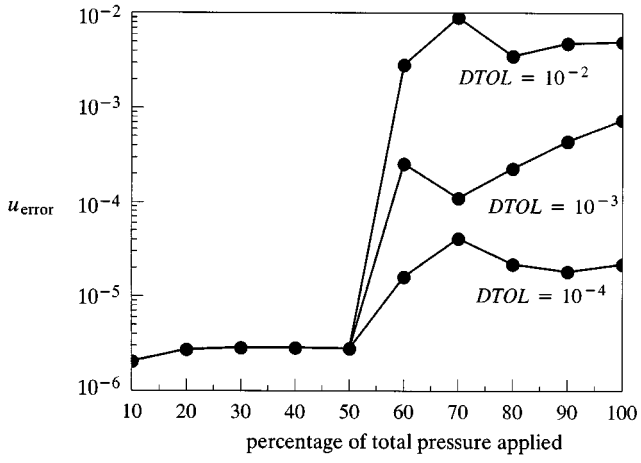

Figure 20. Variation of displacement load path error with load level for undrained loading of a thick cylinder

initially chooses large subincrements in the elastic range and then reduces the step size after the onset of plasticity.

The variation of the time-stepping error as the cylinder is loaded, for runs with 10 coarse time steps and various values of $DTOL$, is shown in Figure 20. In this plot, initial plastic yielding of the cylinder occurs at $q/c' = 0{\cdot}65$ which corresponds to 54 percent of the total pressure applied. Prior to this threshold being reached, the behaviour is elastic and the algorithm does not need to subincrement the coarse load steps. This results in a constant value of the time-stepping error which is independent of $DTOL$. After the onset of plastic yielding, the time-stepping error in the displacements grows to a level which is close to the desired tolerance.

In the case of the drained analysis of the thick cylinder, a much slower loading rate of $\omega = 10^{-2}$ is used to apply the internal pressure. As in the undrained example, the automatic algorithm is employed to predict the response using 1 and 10 coarse time steps with tolerances of 10^{-2}, 10^{-3} and 10^{-4}. Results for these analyses are summarized in Table X. The observations to be made from these statistics are similar to those made for the undrained case, except that roughly double the number of substeps are required and the proportion of failed substeps is smaller.

Figure 18 indicates the drained numerical deformation response for the case of a single coarse load step with $DTOL = 10^{-2}$. This is in good agreement with the analytical solution of Yu[15] over all of the loading range and accurately predicts the exact collapse pressure. As in the undrained case, some oscillations are observed immediately after the onset of plastic yielding, but these may be eliminated by using a smaller value of $DTOL$. Figure 21 illustrates the time-stepping errors in the displacements for the runs using 10 coarse load steps and various values of $DTOL$. Under drained conditions, initial yielding occurs at $q/c' = 0{\cdot}58$ which corresponds to 56·8 per cent of the

Table X. Results for drained loading of thick cylinder using automatic scheme and uniform size coarse increments

$DTOL$	No. coarse time increments	No. subincrements		No. iterations			CPU time (s)
		Successful	Failed	Successful steps	Failed steps	Max	
10^{-2}	1	38	15	92	49	9	3·19
	10	41	12	101	30	4	3·45
10^{-3}	1	115	33	267	99	9	7·53
	10	116	25	267	68	4	7·32
10^{-4}	1	411	97	815	209	9	19·8
	10	421	103	834	210	3	20·6

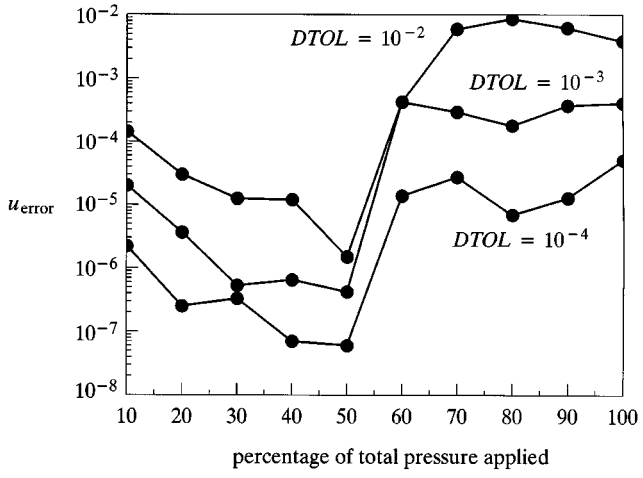

Figure 21. Variation of displacement load path error with load level for drained loading of a thick cylinder

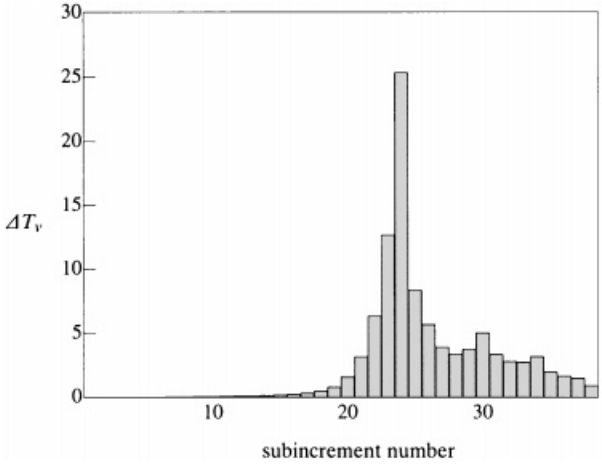

Figure 22. Subincrement selection for drained loading of thick cylinder

total applied pressure. Prior to this point, where the behaviour is elastic, the automatic scheme chooses very small subincrements, which causes the time-stepping errors to lie well below their desired tolerances. These small substeps are clearly seen in Figure 22, which shows a bar chart of the size of each substep. The use of such small subincrements in the elastic range is surprising, but is explained by the fact that the numerical response is always undrained in the first load step. This may be seen from the governing finite element equations, and is a direct consequence of assuming that the initial displacements and pore pressures are equal to zero at $t = 0$. The net result of this is that the automatic scheme adopts small steps during the transition from the undrained state to the drained state, after which it behaves as expected. This phenomenon occurs only when a consolidation analysis is performed with an extremely slow loading rate in an effort to mimic drained behaviour. Following the onset of plastic yielding, the time-stepping errors shown in Figure 21 are very close to their desired tolerances.

3.2. Undrained analysis of flexible strip footing

The intent of this section is to investigate the ability of the consolidation formulation to predict the undrained deformation response, and hence the ultimate collapse load, for a smooth flexible strip footing. The study is motivated by the work of Small[13] who noted that a Biot consolidation formulation, when used with a simple elastoplastic Mohr–Coulomb model, is unable to model undrained behaviour accurately unless a zero dilation angle is used. This observation follows from the fact that a finite dilation angle inevitably causes a drop in the excess pore pressure, and a consequent gain in strength, upon plastic shearing. In finite element consolidation analysis, this effect is manifested by a 'hardening' deformation response which does not exhibit a precise failure load or agree with the predictions from a simple elastoplastic computation.

The finite element mesh and boundary conditions used to model the flexible strip footing are shown in Figure 23. The drained Mohr–Coulomb parameters assumed in the consolidation analyses are

$$E'/c' = 200, \quad \nu' = 0{\cdot}3, \quad \phi' = 20^\circ, \quad \psi' = 0^\circ - 20^\circ$$

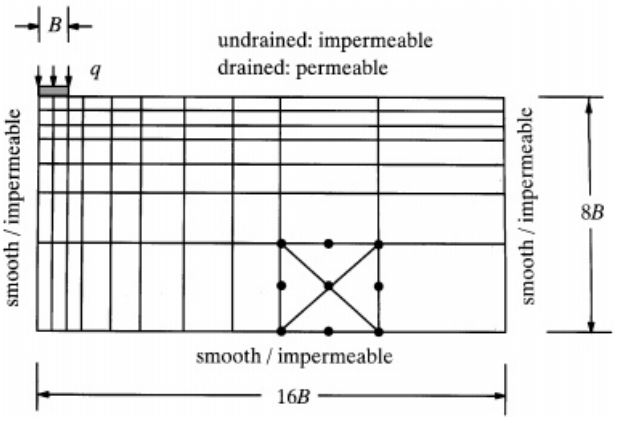

Figure 23. Flexible strip footing on elastoplastic layer

The conventional elastoplastic analysis for this problem models undrained behaviour using a rounded Tresca yield criterion with a zero friction angle and a zero dilatancy angle. From equations (4) and (5), it follows that the undrained parameters for this case must be set as

$$E_u/c_u = 245{\cdot}6, \quad v_u = 0{\cdot}499, \quad \phi_u = 0^\circ, \quad \psi_u = 0^\circ$$

The undrained collapse pressure for the footing is given by the well-known Prandtl formula $q/c_u = 5{\cdot}14$ (or $q/c' = 4{\cdot}83$), where q denotes the applied pressure on the footing. For the consolidation analyses, the rate at which the load is imposed on the footing is defined in terms of the dimensionless quantity

$$\omega = \frac{\Delta q/c'}{\Delta T_{v2}} \tag{6}$$

where the time factor is

$$\Delta T_{v2} = \frac{c_{v2}\Delta t}{B^2} \tag{7}$$

In the above equation, c_{v2} is the two-dimensional consolidation coefficient defined by

$$c_{v2} = \frac{kE'}{2\gamma_w(1+v')\ (1-2v')}$$

and B is the half-width of the footing.

The undrained response of the footing, obtained from a conventional elastoplastic analysis, is shown in Figure 24. This solution clearly asymptotes toward the exact collapse pressure of $q = 4{\cdot}83c' = 5{\cdot}14c_u$ and may be compared against the results of various consolidation analyses which are also plotted. The latter were performed using the automatic scheme with a rapid loading rate of $\omega = 150$ to simulate undrained conditions. In the special case of $\psi' = 0^\circ$, the consolidation analysis was run with the initial stiffness algorithm, an iteration tolerance of $ITOL = 10^{-4}$, and displacement tolerance of $DTOL = 10^{-2}$. This solution closely matches that from the conventional undrained analysis and accurately predicts the exact collapse pressure of

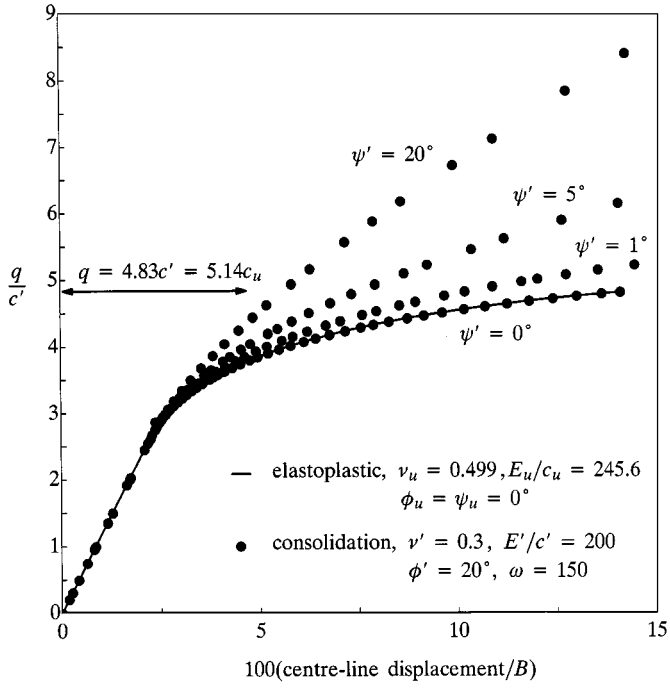

Figure 24. Pressure versus displacement for undrained loading of flexible strip footing on elastoplastic layer

$q = 5{\cdot}14c_u$. The analyses for the remaining dilation angles of 1, 5 and 20° were conducted using tangent stiffness iteration with tolerances of $ITOL = 10^{-6}$ and $DTOL = 10^{-3}$. No detailed statistics for these runs are presented, but they typically generated between 100 and 200 time steps when performed with a single coarse time step. Figure 24 confirms the findings of Small,[13] who concluded that consolidation analyses with a non-zero dilation angle may seriously overstimate the undrained collapse load. Even for a dilation angle of 5°, there is a noticeable 'hardening' of the load–deformation response with no discernible point of failure.

3.3. Consolidation of flexible strip footing with associated flow rule

All of the elastoplastic problems considered so far in this paper have been concerned with the material response over the loading range only. No cases have been analysed in which the load is applied and then held constant while consolidation takes place. This section is concerned with the consolidation behaviour of a smooth flexible strip footing resting on an elastoplastic layer. The layer is modelled by a rounded Mohr–Coulomb yield criterion with an associated flow rule. Although the inadequacy of such a flow rule was highlighted in the previous example, the analyses are performed to enable a direct comparison of the results with those of Manoharan and Dasgupta.[16] Detailed statistics are given for both the automatic and backward Euler methods, so that their accuracy and efficiency can be compared.

The mesh and material properties are the same as those shown in Figure 23, except that the top boundary is now free to drain and the friction and dilation angles are set to $\phi' = \psi' = 20^\circ$. The load is applied to the footing as a uniform prescribed pressure and is imposed over the initial period of $(T_{v2})_0 = 0{\cdot}01$, where T_{v2} is the time factor defined by equation (7). The subsequent consolidation is modelled up to total time factor of $T_{v2} = 1000$. Unless noted otherwise, all analyses are performed using a total load of $q_0/c' = 10$, where q_0 is the maximum pressure applied to the footing at time $T_{v2} = (T_{v2})_0$. The reference solutions for this case were again computed using the second-order scheme of Thomas and Gladwell.[4] These analyses used 1000 equal size time steps over each log cycle of the time factor and an iteration tolerance of $ITOL = 10^{-7}$. The time factor increments adopted for each log cycle are shown in Table XI.

In the first series of runs with the automatic scheme, three different load levels are analysed using a displacement tolerance of $DTOL = 10^{-2}$. The load levels of $q_0/c' = 5$, $q_0/c' = 10$ and $q_0/c' = 15$ are all applied to the footing in a single coarse step. A single coarse step is also used to model the subsequent consolidation. Detailed statistics for these analyses, and a plot of their corresponding transient displacements, are shown in Table XII and Figure 25, respectively. The latter indicates that the numerical settlement predictions from the automatic method are almost identical to the finite element results recently published by Manoharan and Dasgupta.[16] These authors used a mesh composed of 8-noded quadrilaterals with a total of 70 elements and 245 nodes. The mesh shown in Figure 23 was constructed from their model by replacing each quadrilateral with four triangles to give a grid of 280 elements and 595 nodes.

Even when it is used with a single coarse load step to model the loading and consolidation phases of the footing, the automatic scheme generates few failed substeps. Table XII indicates that the ratio of failed to successful steps is 12–14 per cent, which is an acceptable rejection rate for practical computations. Interestingly, all of the failures occur in the loading phase and are primarily generated when the algorithm tries to establish an initial step size.

The iteration counts presented in Table XII highlight the effectiveness of combining the automatic step control mechanism with the Newton–Raphson solution strategy. Each successful substep requires, on average, about five iterations. Not surprisingly, the average number of iterations for failed substeps is greater than this due to the fact that these steps usually occur when the plastic strain increments are large. Since the average number of iterations for a failed substep is about seven, and the maximum number of iterations for any substep always exceeds ten, the

Table XI. Log cycles for analysis of elastoplastic strip footing

	Time factor increment (ΔT_{v2})	Total time factor (T_{v2})
Loading	0·001	0·001
	0·009	0·01
Consolidation	0·09	0·1
	0·9	1·0
	9·0	10·0
	90·0	100·0
	900·0	1000·0

Table XII. Results for strip footing using automatic scheme with two coarse time increments and $DTOL = 10^{-2}$

q_0/c'	No. subincrements		No. iterations			CPU tiime(s)
	Successful	Failed	Successful	Failed	Max	
5	13 + 30 = 43	6 + 0 = 6	51 + 88 = 139	42 + 0 = 42	13	113
10	17 + 27 = 44	6 + 0 = 6	78 + 102 = 180	35 + 0 = 35	12	167
15	21 + 30 = 51	6 + 0 = 6	101 + 164 = 265	39 + 0 = 39	11	273

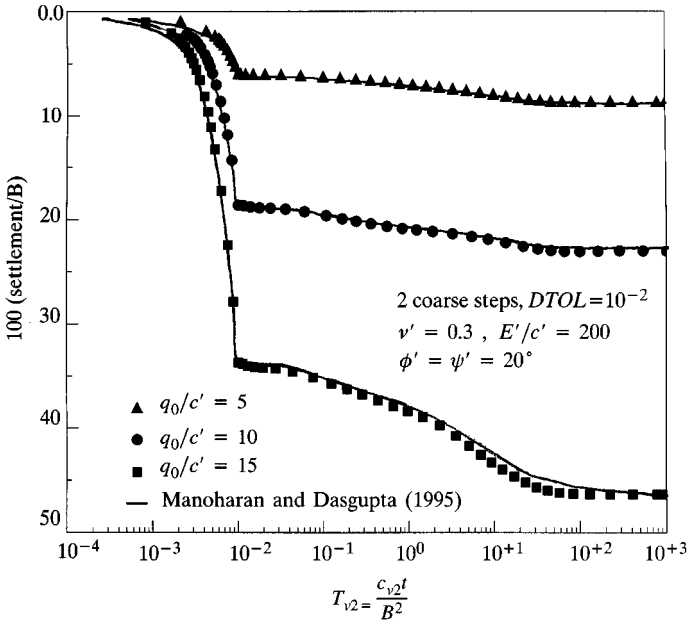

Figure 25. Settlement versus time factor for elastoplastic strip footing

efficiency of the automatic scheme would be improved considerably by setting the maximum iteration limit, *MAXITS*, to about five. As discussed in Section 3, *MAXITS* is currently set to a large number in this paper so that it does not interfere with the step size predicted by the local error estimator.

The distribution of subincrement sizes for the analysis with $q_0/c' = 10$ is shown in Figure 26. As expected, the smallest substep of $\Delta T_{v2} = 1{\cdot}3 \times 10^{-4}$ occurs during the loading phase, where the changes in the deformations and pore pressures are rapid. The substeps are also small immediately after the maximum load is reached, but then grow quickly once the excess pore pressures are partially dissipated. Toward the end of the consolidation period, where the excess pore pressures are close to zero, the automatic scheme selects the largest time step of $\Delta T_{v2} = 403$. Thus, over the total consolidation interval considered, the time step is increased by more than six orders of magnitude. Time step distributions such as the one indicated in Figure 26 are difficult to select by hand, and would not be obvious even to an experienced analyst.

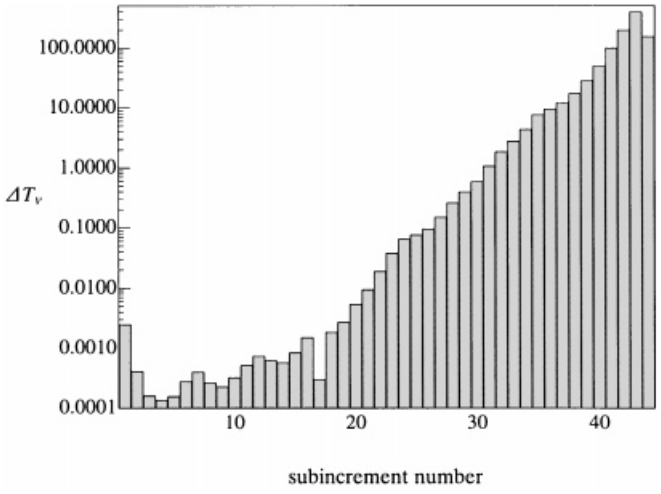

Figure 26. Subincrement size selection for consolidation of elastoplastic strip footing

Table XIII. Results for elastoplastic strip footing using automatic scheme with logarithmic coarse time steps and $q_0/c' = 10$

$DTOL$	No. coarse time incs. per log cycle	No. subincrements		No. iterations in successful subincrements	CPU time (s)
		Successful	Failed		
10^{-2}	1	$19 + 30 = 49$	$5 + 0 = 5$	$83 + 114 = 197$	163
10^{-3}	1	$51 + 58 = 109$	$5 + 0 = 5$	$158 + 167 = 325$	215
10^{-4}	1	$193 + 149 = 342$	$25 + 3 = 28$	$429 + 342 = 771$	485

To further investigate the performance of the automatic scheme, the footing was analysed for the case of $q_0/c' = 10$ with a range of displacement tolerances and a logarithmically varying set of coarse time steps. The latter are listed in Table XI and the results from these runs are shown in Table XIII. For the case of $DTOL = 10^{-2}$, the automatic scheme generates 49 successful substeps, 5 failed substeps, and uses 163 s of CPU time. With the same value of $DTOL$, but using two coarse time steps, the corresponding statistics, shown in Table XII, are 44 successful steps, 6 failed steps and 167 s of CPU time. This comparison again confirms that the performance of the automatic scheme is largely independent of the size and distribution of the initial coarse time steps. The data in Table XIII shows that reducing the error tolerance $DTOL$ reduces the average number of iterations required for each time step. This is expected, as smaller values of $DTOL$ lead to smaller time steps. In this example, cutting $DTOL$ from 10^{-2} to 10^{-4} results in the average number of iterations being decreased from just under four to just over two. For the same reason, smaller values of $DTOL$ also lead to a reduced proportion of failed subteps. These two effects explain why the CPU time does not increase dramatically when $DTOL$ is tightened by an order of magnitude. The time-stepping errors in the displacements for each of the analyses in Table XIII are plotted in Figure 27. For all values of $DTOL$, the automatic scheme again successfully constrains the error to an approximately constant value which lies near the desired tolerance.

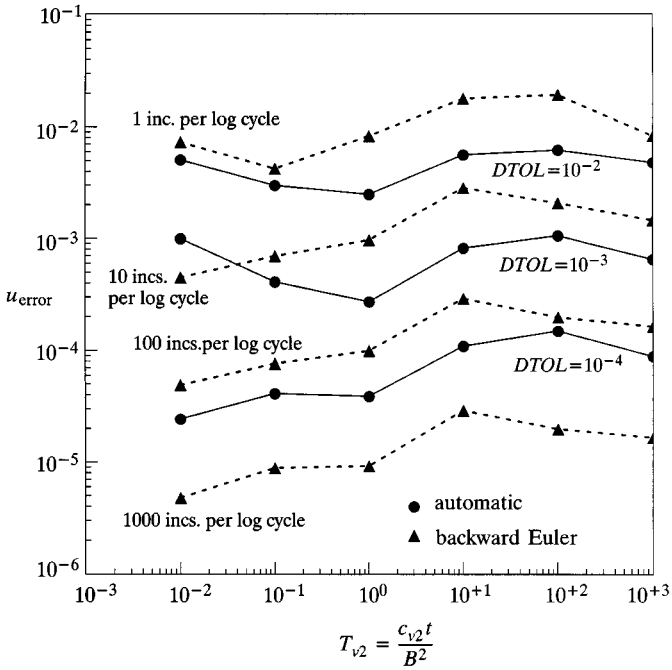

Figure 27. Temporal discretization error in displacements versus time factor for elastoplastic strip footing (logarithmic coarse time steps)

Table XIV. Backward Euler results for elastoplastic strip footing using logarithmic increment sizes

No. increments per log cycle		Total No. increments	No. of iterations		CPU time (s)
Loading	Consol.		Total	Max.	
1	1	1 + 6 = 7	25 + 33 = 58	23	88
10	10	10 + 60 = 70	72 + 145 = 217	7	153
100	100	100 + 600 = 700	367 + 917 = 1284	4	727
1000	1000	1000 + 6000 = 7000	2564 + 5180 = 7744	3	4370

To assess the performance of a more traditional solution method, the footing response is now analysed using the backward Euler scheme for the load case of $q_0/c' = 10$. In this example, the time factor increments, listed in Table XI, are subdivided using 1, 10, 100 and 1,000 equal-size intervals to give the time steps shown in Table XIV. The results for these analyses, also summarized in Table XIV, show that the Newton–Raphson scheme may require a large number of iterations if the time discretization is very coarse. For the crudest analysis with one time step in the loading phase and six time steps in the consolidation phase, up to 23 iterations are needed to reach convergence and the average iteration count is just over eight. This is in contrast to the 7000 increment run which gives maximum and average iteration counts of three and one, respectively. As expected, the largest average iteration counts for all the analyses occur during the loading phase. Figure 27 summarizes the temporal discretization error at the end of each log cycle of the

time factor for the various runs. This plot indicates that, even with the crudest discretization of one time step per log cycle, the backward Euler method gives a time-stepping error of just two percent. The results also confirm the expected first-order accuracy of this type of solution strategy.

The results in Tables XIII, XIV and Figure 27 can be used to compare the relative efficiency of the automatic and backward Euler methods for the footing problem. The figure indicates that these two schemes, when used with $DTOL = 10^{-2}$ and one increment per log cycle, respectively, give similar maximum time stepping errors. The CPU time for the backward Euler method, however, is only 88 s as opposed to 163 s for the automatic scheme. For more accurate analyses, the relative performance of the automatic scheme improves significantly and is competitive with that of the backward Euler algorithm. This can be seen by comparing the timing statistics for the automatic analysis with $DTOL = 10^{-4}$ against the timing statistics for the 700 increment backward Euler run. The former, although marginally more accurate, requires only 485 CPU s as opposed to 727 CPU s for the latter, a saving of approximately 33 per cent. When making this type of comparison, it should be remembered that the backward Euler scheme will usually need to be run with a range of different time steps in order to determine when the time-stepping error is negligible. The automatic scheme, however, need only be run once.

3.4. Consolidation of flexible strip footing with non-associated flow rule

The results shown in Section 3.2 highlighted the need to employ a non-associated flow rule when using a simple Mohr–Coulomb model with a Biot consolidation formulation. In particular, it is necessary to use a non-dilatant flow rule to obtain solutions which match those from a conventional elastoplastic analysis for the limiting case of undrained loading. This section examines the ability of the consolidation formulation to accurately predict the drained collapse pressure for a flexible strip footing subjected to a very slow rate of loading. The important influence of the iteration tolerance on the efficiency of the initial stiffness algorithm is also investigated.

The geometry, boundary conditions and finite element mesh for the footing are identical to those used in the preceding example (see Figure 23). The drained soil parameters adopted for the rounded Mohr–Coulomb model are similar to those employed in Section 3.2, except that the dilation angle is always zero. Thus

$$E'/c' = 200, \quad v' = 0.3, \quad \phi' = 20^\circ, \quad \psi' = 0^\circ$$

and the corresponding Prandtl collapse pressure $q_0/c' = 14{\cdot}83$. The conventional elastoplastic analysis for this problem uses the above parameters, and the rounded Mohr–Coulomb yield surface, to model the drained state. One thousand equal-size pressure increments are imposed on the footing and an initial stiffness algorithm is employed to solve the governing equations.

The consolidation analyses are performed with loading rate values ranging from $\omega = 0{\cdot}015$ to $\omega = 150$, where ω is again defined by equation (6). The former case generates very small excess pore pressures and thus models the drained condition very closely. As shown in Section 3·2, the higher rate accurately simulates undrained loading. All of the consolidation runs are performed with two coarse load steps, $DTOL = 10^{-2}$, and an initial stiffness iteration tolerance of $ITOL = 10^{-4}$.

The results for the various analyses, shown in Figure 28, indicate that the drained pressure–displacement responses from the consolidation and conventional elastoplastic methods are in

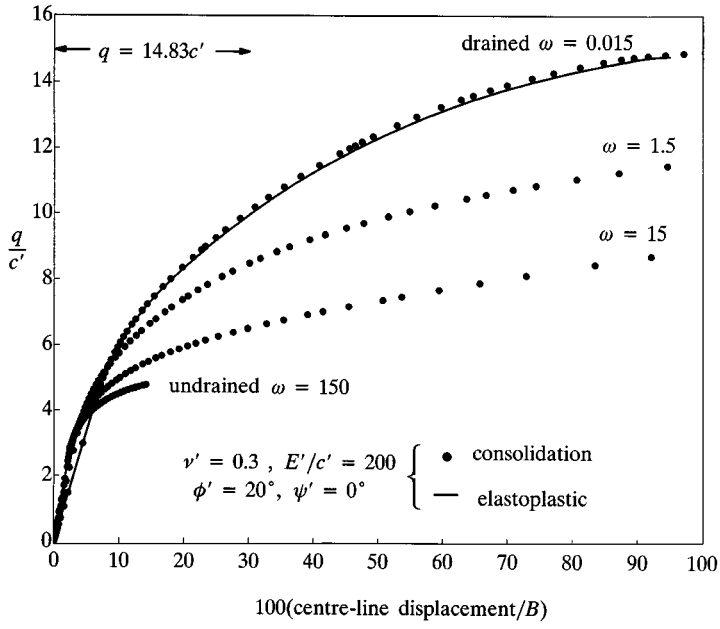

Figure 28. Pressure versus displacement for flexible strip footing on elastoplastic layer with varying load rates

close agreement over all the loading range. Both techniques accurately predict the Prandtl collapse pressure of $q_0/c' = 14{\cdot}83$, which is valid for a soil with an associated flow rule. As expected, the consolidation results give a stiffer response as the loading rate is reduced. For the undrained case, which is modelled using the maximum loading rate of $\omega = 150$, the results are the same as those discussed in Section 3.2.

As mentioned previously, the initial stiffness variant of the consolidation algorithm is useful for soil models which involve non-associated flow rules, where the tangent stiffness matrix may become ill-conditioned. When performing consolidation analyses with the initial stiffness method, the setting of the iteration tolerance $ITOL$ has a dramatic effect on the total CPU time. It is natural to suggest that the value of this parameter should, in some way, be linked to the value of $DTOL$, since there is little sense in performing very accurate iterations if the chief source of error is due to the use of large time steps. To investigate this question, the footing problem described above is analysed using a range of iteration tolerances. The geometry, boundary conditions and mesh are unchanged, as are the material properties. The only difference is that the maximum load of $q_0/c = 4{\cdot}2$ is now applied over the time step $\Delta T_{v2} = 0{\cdot}01$ and consolidation is allowed to take place until $T_{v2} = 1000$. In addition, one step per log cycle is used to specify the size of each initial coarse time increment. The reference displacements for this case are obtained using the automatic scheme with tolerances of $ITOL = 10^{-7}$ and $DTOL = 10^{-6}$. These results contain very small time-stepping errors because of the large number of time steps that are generated.

The results of the iteration study for the footing are summarized in Table XV. Data are presented for $DTOL$ settings of 10^{-2}, 10^{-3} and 10^{-4}, with each of these tolerances being analysed for a range of $ITOL$ values. Because the rate of convergence of the initial stiffness method is only linear, the iteration tolerance is observed to have a marked influence on the CPU

Table XV. Results for strip footing on non-associated layer using automatic scheme with initial stiffness iteration

DTOL	*ITOL*	No. subincrements		No. iterations in successful subincrements	CPU time (s)
		Successful	Failed		
10^{-2}	10^{-2}	$15+47=62$	$5+3=8$	$20+48=60$	99
	10^{-3}	$18+41=59$	$6+0=6$	$109+83=192$	146
	10^{-4}	$19+38=57$	$7+0=7$	$325+116=441$	276
	10^{-5}	$19+38=57$	$7+0=7$	$670+234=904$	497
10^{-3}	10^{-3}	$50+72=122$	$11+0=11$	$65+95=160$	130
	10^{-4}	$52+71=123$	$13+0=13$	$323+148=471$	191
	10^{-5}	$53+71=124$	$15+0=15$	$1051+204=1255$	342
	10^{-6}	$53+71=124$	$16+0=16$	$2108+308=2416$	557
10^{-4}	10^{-4}	$264+184=448$	$90+5=95$	$346+325=671$	496
	10^{-5}	$203+175=378$	$59+1=60$	$1189+393=1582$	526
	10^{-6}	$206+173=379$	$59+0=59$	$3936+501=4437$	866
	10^{-7}	$207+173=380$	$50+0=50$	$8250+721=8971$	1356

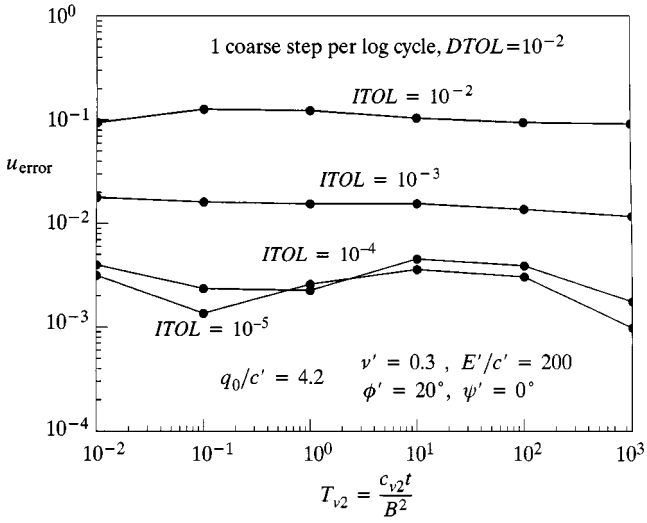

Figure 29. Temporal discretization error in displacements versus time factor for elastoplastic strip footing using automatic algorithm and initial stiffness iteration

times recorded. In the case with $DTOL = 10^{-2}$, for example, the CPU time increases from 99 s for $ITOL = 10^{-3}$ to 497 s for $ITOL = 10^{-5}$. Similar growth factors are observed for all other values of $DTOL$ considered. The extra expense incurred by using a stringent iteration tolerance is justified only if the accuracy of the resulting solution is greatly improved. To investigate whether this is the case, plots of the errors for the analyses with $DTOL$ equal to 10^{-2} and 10^{-3} are shown, respectively, in Figures 29 and 30. Both of these plots demonstrate that the displacement error

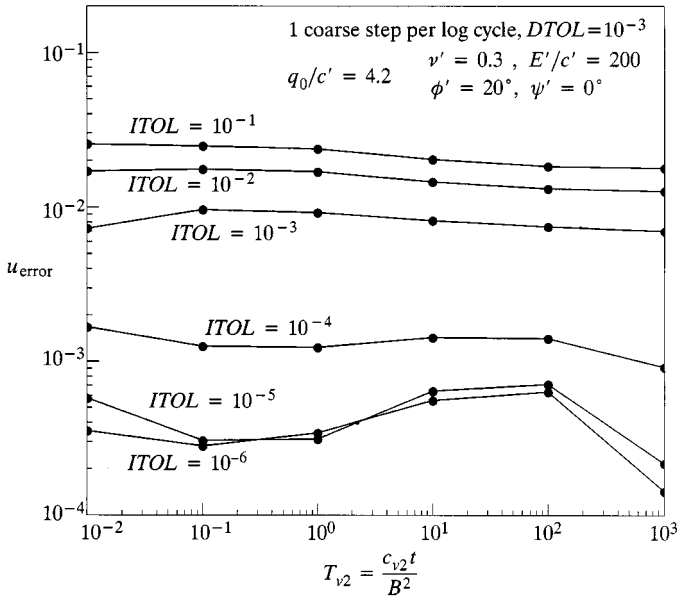

Figure 30. Temporal discretization error in displacements versus time factor for elastoplastic strip footing using automatic algorithm and initial stiffness iteration

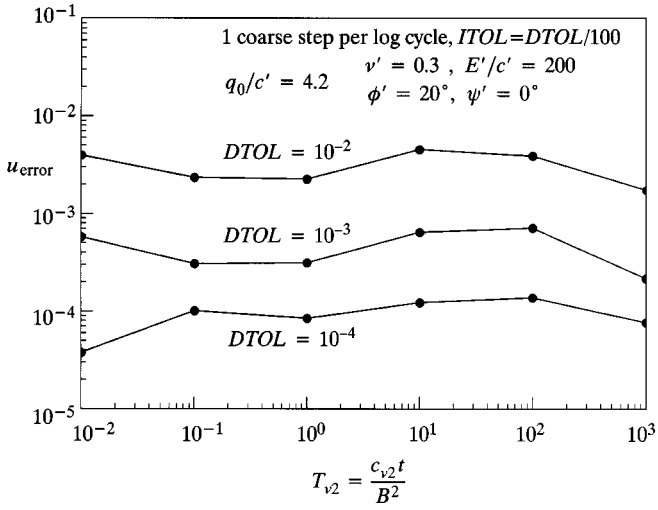

Figure 31. Temporal discretization error in displacements versus time factor for elastoplastic strip footing using automatic algorithm and initial stiffness iteration

does not continue to decrease as the iteration tolerance is tightened. In the analysis with $DTOL = 10^{-2}$, for example, there is no consistent improvement in the accuracy of the analysis once $ITOL$ is reduced below a value of around $ITOL = 10^{-4}$. Similarly, for $DTOL = 10^{-3}$, there is no discernible reduction in the displacement error for iteration tolerances tighter than 10^{-5}.

These results suggest that the time-stepping error typically reaches a minimum value when $ITOL \approx DTOL/100$. Choosing a value below this threshold does not reduce the overall solution error, and only serves to increase the CPU time. The results for various runs with $ITOL$ set to $DTOL/100$ are shown in Figure 31. In all cases, the displacement error is held approximately constant over the consolidation interval and lies near the desired tolerance $DTOL$. Although no results are presented here, this method of setting the iteration tolerance has also been found to work well for consolidation analyses which employ Newton–Raphson iteration.

4. CONCLUSIONS

The automatic time incrementation scheme described in Reference 1 has been used successfully to predict the behaviour of a number of problems involving the consolidation of elastic and elastoplastic materials. These applications prove that the proposed algorithm is not only robust and efficient, but also able to constrain the temporal discretization error to lie near a desired tolerance. A major advantage of the new algorithm is that it removes the need to select the time increments in consolidation analysis by trial and error. Moreover, the behaviour of the scheme is largely insensitive to the size and distribution of the coarse time steps that are required to start the analysis.

The pitfalls of adopting an associated Mohr–Coulomb model in consolidation analysis have been highlighted. For rapid rates of loading, the yield surface should be used with a non-associated flow rule and a zero angle of dilatancy to obtain sensible predictions of soil behaviour.

Finally, it was shown that there is little benefit in using excessively stringent iteration tolerances in elastoplastic consolidation calculations. For the automatic scheme, a simple rule is proposed which ties the value of the iteration tolerance to the displacement error tolerance. This rule helps to minimize the number of wasted iterations, yet ensures that the desired accuracy requirements are met.

REFERENCES

1. S. W. Sloan and A. J. Abbo, 'An automatic time stepping scheme for elastic and elastoplastic consolidation. Part 1: Theory and implementation', *Int. J. Numer. Anal. Meth. Geomech.*, **6,** 467–492 (1999).
2. M. B. Reed, 'An investigation of numerical errors in the analysis of consolidation by finite element analysis', *Int. J. Numer. Anal. Meth. Geomech.*, **8,** 243–257 (1984).
3. W. Kanok-Nukulchal and V. W. Suaris, 'An efficient finite element scheme for elastic porous media', *Int. J. Solids Struct.*, **48,** 37–49 (1982).
4. R. M. Thomas and I. Gladwell, 'Variable-order variable step algorithms for second-order systems. Part 1: The methods', *Int. J. Numer. Meth. Engng.*, **26,** 39–53 (1988).
5. M. E. Laursen and M. Gellert, 'Some criteria for numerically integrated matrices and quadrature formulas for triangles', *Int. J. Numer. Meth. Engng.*, **12,** 67–76 (1978).
6. K. Terzaghi, 'Die Berechnung der Durchlassigkeitsziffer des Tones aus dem Verlauf der hydrodynamischen Spannungsersceinungen', Originally published in 1923 and reprinted in *From Theory to Practice in Soil Mechanics*, Wiley, New York, 1960, pp. 133–146.
7. R. S. Sandhu, H. Lui and K. J. Singh, 'Numerical performance of some finite element schemes for analysis of seepage in porous elastic media', *Int. J. Numer. Anal. Meth. Geomech.*, **1,** 177–194 (1977).
8. P. A. Vermeer and A. Verruijt, 'An accuracy condition for consolidation by finite elements', *Int. J. Numer. Anal. Meth. Geomech.*, **5,** 1–14 (1981).
9. J. Mandel, 'Consolidation des sols', *Geotechnique*, **III,** 287–299 (1953).
10. J. R. Booker, 'The consolidation of a finite layer subject to surface loading', *Int. J. Solids Struct.*, **10,** 1053–1065 (1974).

11. A. J. Abbo and S. W. Sloan, 'A smooth hyperbolic approximation to the Mohr-Coulomb yield criterion', *Comput. Struct.*, **54,** 427–441 (1995).
12. A. J. Abbo, '*Finite element algorithms for elastoplasticity and consolidation*', Ph.D. Thesis, University of Newcastle, Australia, 1997.
13. J. C. Small, '*Elasto-plastic consolidation of Soils*', Ph.D. Thesis, University of Sydney, 1977.
14. R. Hill, 'The Mathematical Theory of Plasticity, Clarendon Press, Oxford, 1950.
15. H. S. Yu, 'Expansion of a thick cylinder of soil', *Comput. Geotech.*, **14,** 21–41 (1992).
16. N. Manoharan and S. P. Dasgupta, 'Consolidation analysis of elastoplastic soil', *Comput. Struct.*, **54,** 1005–1021 (1995).

